Enrico Silva, Nicola Pompeo, and Oleksandr V. Dobrovolskiy

8 Vortices at microwave frequencies

Abstract: The behavior of vortices at microwave frequencies is an extremely useful source of information on the microscopic parameters that enter the description of the vortex dynamics. This feature has acquired particular relevance since the discovery of unusual superconductors, such as cuprates. Microwave investigation then extended its field of application to many families of superconductors, including the artificially nanostructured materials. It is then important to understand the basics of the physics of vortices moving at high frequency, as well as to understand what information the experiments can yield (and what they can not). The aim of this Chapter is to introduce the readers to the physics of vortices under a microwave electromagnetic field, and to guide them to an understanding of the experiment, also by means of the illustration of some relevant results.

Keywords: vortices, microwave frequency, pinning

8.1 Introduction

When dealing with vortices in a microwave electromagnetic (henceforth, e.m.) field, one necessarily deals with vortex dynamics. Thus, the focus is on the e.m. response of moving vortices. Microwave frequencies, broadly in the range $1 \div 100$ GHz, correspond to a wavelength in vacuum of several cm. Then, in most cases the detected signal in experiments comes from the average motion of a very large amount of vortices ($n = B/\Phi_0$ per unit area). This aspect immediately brings a common feature to many of the existing models for microwave vortex motion: the models are usually based upon a *single-vortex equation of motion*, which contains some phenomenological parameters. On the basis of the equation of motion, a response function is derived (the complex resistivity, or conductivity, or surface impedance). From the experiments one deduces the averaged phenomenological parameters. Then, a connection with the microscopic theory is attained at the level of the parameters. While exceptions exist and more complex models have been developed, in this Chapter we will describe the microwave response of moving vortices in this restricted (but most common) meaning.

In the previous Chapters 3, 5, and 9 the reader was introduced to the vortex dynamics, in particular from the point of view of the motion of vortices under the effect

Enrico Silva, Dipartimento di Ingegneria, Università Roma Tre, Via Vito Volterra 62, I-00146, Roma, Italy, e-mail: enrico.silva@uniroma3.it
Nicola Pompeo, Dipartimento di Ingegneria, Università Roma Tre, Via Vito Volterra 62, I-00146, Roma, Italy, e-mail: nicola.pompeo@uniroma3.it
Oleksandr V. Dobrovolskiy, Physikalisches Institut, Goethe-Universität, Max-von-Laue-Str. 1, D-60438 Frankfurt am Main, Germany, email: dobrovolskiy@physik.uni-frankfurt.de

DOI 10.1515/9783110456806-009,

of a steady dc current density $\boldsymbol{J}$. The vortex is subjected to the so-called " Lorentz force" (per vortex unit length):[1]

$$\boldsymbol{f}_L = \boldsymbol{J} \times \Phi_0 \tag{8.1}$$

When the current density exceeds the critical current density, the vortices move with average velocity $\boldsymbol{v}$. The overall motion of all vortices constituting the flux density $\boldsymbol{B}$, gives rise to the electric field:

$$\boldsymbol{E} = \boldsymbol{B} \times \boldsymbol{v} \tag{8.2}$$

and hence to a finite dissipation, since in general $\boldsymbol{J} \cdot \boldsymbol{E} \neq 0$. Natural and artificial defects act as pinning centers for vortices, and can stop the motion. When the pinning recall becomes irrelevant (due, e.g., to a sufficiently large J or to large thermal activation), vortices are completely free to move in a steady motion, reaching the so-called flux-flow regime. In this regime, the environment exerts a force that can be written as a viscous drag [1], so that $\boldsymbol{f}_{\text{env}} = -\eta \boldsymbol{v}$. This relation defines the phenomenological parameter η, the so-called vortex viscosity or viscous drag coefficient. This is one of the key parameters in the description of the vortex motion.

Pinning is the second important process that has to be considered. The overall pinning effect can be described in terms of a local pinning potential $U(\boldsymbol{r}, B)$. Vortices tend to occupy the pinning potential minima of U; any displacements from these equilibrium positions give rise to a restoring force on the vortex. Thus, there exists an elementary pinning force (per unit length) on the vortex:

$$\boldsymbol{f}_p = -\nabla U \simeq -k_{\text{p}} \boldsymbol{u} \tag{8.3}$$

where $\boldsymbol{u}$ is the displacement of the vortex from the equilibrium position, and the latter approximate equality holds in the limit of small displacement[2] and it defines the pinning constant (or Labusch parameter) k_{p}. It should be mentioned that, in anisotropic superconductors, the e.m. problem is much more complicated, since the vortex displacement $\boldsymbol{u}$ (or the velocity $\boldsymbol{v} = \dot{\boldsymbol{u}}$) are not necessarily parallel to the forces [3]. We will not address this issue explicitly, the reader is referred to the specific literature [3, 4].

Finally, the thermal activation can be treated by formally adding a thermal stochastic force, $\boldsymbol{f}_{\text{th}}$ to the Lorentz force. One then has the equation of motion for a single vortex:

$$m\ddot{\boldsymbol{u}} = \boldsymbol{f}_L + \boldsymbol{f}_{\text{th}} - \eta \dot{\boldsymbol{u}} - k_{\text{p}} \boldsymbol{u} \tag{8.4}$$

where we have neglected the Hall terms. An extended discussion on the validity of this approximation can be found in [5].

1 The force per unit length should not be confused with the pinning force $\boldsymbol{F}_p$ used in the treatment of pinning, which is a force per unit volume. The latter is introduced when the elementary pinning forces (per unit length) $\boldsymbol{f}_{\text{p}}$ are summed (Chapter 5), which is conceptually analogous to the passage from the single-vortex equation (8.1) to the electric field equation (8.2).

2 For recent results on the applicability of the elastic approximation, see [2].

The explicit models that are used to describe flux flow, pinning, and thermal activation define the final framework that will be used to analyze the experiments. A complete review of the various models is well beyond the scope of this introductory Chapter, but it is nevertheless useful to introduce some remarks.

The vortex viscosity η is the parameter that characterizes the free vortex flow. The microscopic origin of η was first addressed by Bardeen and Stephen (BS) [6] for s-wave conventional superconductors, in the following framework: the power dissipated per vortex unit length, $W = \boldsymbol{f}_{\text{env}} \cdot \boldsymbol{v} = \eta v^2$, is transferred to normal currents, flowing inside vortex cores (modeled as fully normal cylinders with radius $\sim \xi$) and closing outside. These currents give a Joule dissipated power $\sim v^2 \Phi_0^2 / 2\pi\xi^2 \rho_n$ (ρ_n is the normal state resistivity), whence:[3]

$$\eta = \frac{\Phi_0 B_{c2}}{\rho_n} \tag{8.5}$$

The BS model is valid for dirty s-wave superconductors. The clean [9] and the general [10, 11] case calculations take into account the full spectrum of the quasiparticle bound states. It is interesting to note that, by combining the general case calculation [10] to the reinstatement of the Hall term in the flux-flow motion [5], one has in a very wide range of regimes:

$$\eta = n_{\text{qp}} \pi \hbar \omega_c \tau_{\text{qp}} \tag{8.6}$$

where ω_c is the cyclotron angular frequency at H_{c2}, and τ_{qp} and n_{qp} are the quasiparticle relaxation time and concentration in the vortex, respectively. Thus, Equation (8.6) is a good general approximation for η, and Equation (8.5) a practical and often used rule of thumb for the order of magnitude of η. We mention that in cuprates (as well as in any superconductors with lines of nodes in the gap) this picture may complicate severely, and additional temperature and field dependences may show up in η [12–14]. It is apparent that η is the vortex parameter most closely linked to the microscopic properties of quasiparticles.

The role of vortex mass is a longstanding and much debated issue that has not found a commonly accepted solution yet. Most estimates [15–18] give a negligible contribution of the inertial term to the overall response, and in the following we will neglect the vortex mass for the microwave frequency range we are interested in (however, some relevance of the inertial term at or above THz frequencies cannot be ruled out).[4]

The treatment of the pinning in terms of a simple elastic recall can be at first considered exceedingly simplified. In many superconductors, and in particular in

3 Note that most microscopic models develop the calculations for η in the low-frequency limit. While in conventional superconductors and in optimally doped $YBa_2Cu_3O_{7-\delta}$ there is no evidence for any frequency dependence of η in the microwave range [7], in underdoped $YBa_2Cu_3O_{6.52}$ this hypothesis has been experimentally questioned [8].

4 In addition, one has to recall that at frequencies higher than the gap breakdown frequency, superconductivity is destroyed. The gap breakdown frequency $\omega_B = 2\Delta(0)/\hbar$ is of the order of 100 GHz for a superconductor with a transition temperature of $T_c \simeq 10$ K.

cuprates, various phases of the vortex matter can exhibit extremely different vortex pinning. For example, the elasticity of the Abrikosov lattice makes few pinning centers very effective in blocking the motion of the whole lattice, while in the vortex liquid phase vortices can only be individually pinned. Pinning is also affected by the flux line tension: a rigid flux line can be pinned by a single pinning center, but (at the other extreme) pancake vortices need to be individually pinned on each distinct layer. In most cases, however, this complexity can be "hidden" into the field and temperature dependencies of appropriate parameters. In particular, at microwave frequencies one encounters the favorable circumstance that the average displacement of the vortex from the equilibrium position in typical experiments is of the order of 0.1 nm or less [19]. In this case, the vortex system can be treated in the local, single-vortex limit, and a single-vortex, mean-field approach is acceptable.

The thermal activation can be treated in a large variety of models. In the specific field of the ac electrodynamics, the most common approaches have been developed by Coffey and Clem (CC) [20] and Brandt [21]. CC exploited the mathematical properties of a uniform sinusoidal pinning potential. Brandt assumed a phenomenological thermally relaxing pinning constant $k_{p,th} = k_p \exp^{-t/\tau}$. In both cases, a vortex characteristic relaxation time was obtained:

$$\tau_{CC} = \tau_p \frac{I_0^2(u) - 1}{I_1(u) I_0(u)} \tag{8.7}$$

for the CC model, where $I_{0,1}$ are modified Bessel functions, $u = U_0/2K_B T$, and U_0 is the height of the sinusoidal pinning potential, while for the Brandt model:

$$\tau_B = \tau_p e^{U_0/K_B T} \tag{8.8}$$

where U_0 is the single pinning well height. In both cases, one defines:

$$\tau_p = \frac{\eta}{k_p} = \frac{1}{\omega_p} = \frac{2\pi}{f_p} \tag{8.9}$$

where the last two equalities define the extremely important vortex parameter, namely the depinning (angular) frequency (also named "pinning frequency").

Putting together all the approximations made up to now, we conclude this Section with the equation of motion that is the starting point for the microwave response of vortices in superconductors. It reads:

$$\eta \dot{\boldsymbol{u}} + k_p \boldsymbol{u} = \boldsymbol{J} \times \Phi_0 + \boldsymbol{f}_{th} \tag{8.10}$$

We stress again that the model described up to now:

- is derived from a single-vortex equation of motion, so that the effect of vortex-vortex interactions must be introduced in an effective fashion in the parameters;
- is obtained in the very small displacement approximation (with respect to pin-pin distance), that holds at sufficiently high frequencies;

- does not contain the Cooper pair or quasiparticle dynamics entirely, so that it is not expected to hold at very high frequency (as a rule of thumb, approaching infrared) or very close to the critical temperature or field;
- is a linear response model: nonlinearities must be treated in a different way.[5]

8.2 Vortex motion complex resistivity

Once the equation of motion for the (single) vortex is obtained, Equation (8.10), it is possible to derive the response function in terms of the electric field arising from the application of an ac current density, that is in the form $\boldsymbol{E} = \rho_{\mathrm{v}}\boldsymbol{J}$, where $\rho_{\mathrm{v}}(T, H, f)$ is the *vortex motion complex resistivity*. In so doing, since we deal with the applied magnetic field $\boldsymbol{H}$ while the vortex response is determined by the flux density $\boldsymbol{B}$, we assume to be in the London limit (that is, not extremely close to H_{c1}), so that $B \simeq \mu_0 H$.

It is instructive to discuss the result first with no thermal forces (no thermal activation, no creep). This model was developed early by Gittleman and Rosenblum (GR) [25] and it is still very successful (with the appropriate redefinition of the vortex parameters). Assuming harmonic current, $\boldsymbol{J}\mathrm{e}^{\mathrm{i}\omega t}$ in Equation (8.10) with $\boldsymbol{f}_{\mathrm{th}} = 0$, solving for the harmonic vortex velocity $\boldsymbol{v}\mathrm{e}^{\mathrm{i}\omega t}$, multiplying by n to add the contribution of all vortices, cross-multiplying by Φ_0 and using Equation (8.2), one finally finds:

$$\rho_{v,GR} = \frac{\Phi_0 B}{\eta + \frac{k_{\mathrm{p}}}{\mathrm{i}\omega}} = \frac{\Phi_0 B}{\eta}\frac{1}{1 - \mathrm{i}\frac{k_{\mathrm{p}}}{\eta\omega}} = \rho_{\mathrm{ff}}\frac{1}{1 - \mathrm{i}\frac{\omega_{\mathrm{p}}}{\omega}} \tag{8.11}$$

where the last equality contains explicitly the depinning frequency (see Equation (8.9)) $f_{\mathrm{p}} = \omega_{\mathrm{p}}/2\pi$ and the *flux-flow resistivity*:

$$\rho_{\mathrm{ff}} = \frac{\Phi_0 B}{\eta} \simeq \rho_n \frac{B}{B_{\mathrm{c2}}} \tag{8.12}$$

Here, the last approximate equality derives from the application of the BS model for η, and it is not required for Equation (8.11) to hold.

Even this simple model highlights several of the powerful features of the microwave experiments. First, there exists at least a characteristic frequency (or, which is the same, a characteristic time scale) in the motion of vortices: below the depinning frequency, $\omega \ll \omega_{\mathrm{p}}$, the response is purely inductive. This regime is also called the "Campbell regime" [26], characterized by the "Campbell resistivity" ρ_{C}, and one has:

$$\rho_{v,GR}(\omega \ll \omega_{\mathrm{p}}) \simeq \mathrm{i}\rho_{\mathrm{C}} = \mathrm{i}\frac{\omega\Phi_0 B}{k_{\mathrm{p}}} \tag{8.13}$$

5 An extension of the CC model to nonlinear response, nonzero Hall coefficient, directional and asymmetric washboard pinning potential, and to the presence of a superimposed dc current has been given by Shklovskij et al. [22–24].

Second, at sufficiently high frequency, $\omega \gg \omega_p$, one has the free flux-flow regime, where $\rho_v \simeq \rho_{ff}$. We note that in this case it becomes possible to measure the flux flow of vortices in the linear regime: this has to be contrasted by typical experiments in dc, where a current larger than the critical (depinning) current must be applied (Chapter 5). Thus, while in dc the flux-flow resistivity is measured in the strongly nonlinear regime, at microwave frequencies it is possible to obtain the same quantity in the linear regime, thus avoiding the serious experimental complications when a large current has to be passed in the superconducting sample.

It is quite clear that a measurement of the complex response (real and imaginary parts) provides at the same time the Campbell and flux-flow resistivities, once the simple GR model is assumed. In this case, a very relevant experimental parameter is the so-called r parameter, defined empirically as:

$$r = \frac{\Im(\rho_v)}{\Re(\rho_v)} = \frac{\omega_p}{\omega} \tag{8.14}$$

where the last equality holds until the GR model, Equation (8.11), holds. The r parameter has been used for a long time [27, 28] to determine the regime of the vortex motion.

This simple model has been very successful in the interpretation of the data in low-T_c superconductors. In particular, the frequency dependence of the microwave power absorbed by vortices in flat PbIn and NbTa sheets at radio and microwave frequencies at fixed magnetic field and temperature was found to exhibit the expected crossover at f_p from the weak dissipation at low frequencies to the strong dissipation at high frequencies [25], as reported in Figure 8.1.

More recent studies in metallic, low-T_c superconductors have explored the dependence of the depinning frequency f_p on the temperature and the magnetic field. It must be stressed that $f_p(H, T) = k_p/\eta$ contains both the fundamental, intrinsic parameters contained in η (Equations (8.5), (8.6)) and the sample-specific pinning

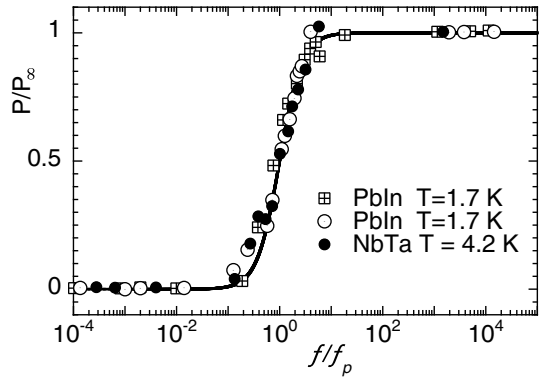

Fig. 8.1: Normalized dissipated power in type-II superconductors at $H = \frac{1}{2}H_{c2}$ as a function of the measuring frequency normalized to f_p (replotted from [25], $f_p = 3.9, 5.1, 15$ MHz) and fit by Equation (8.11) (real part). Note that the normalization simplifies out ρ_{ff}.

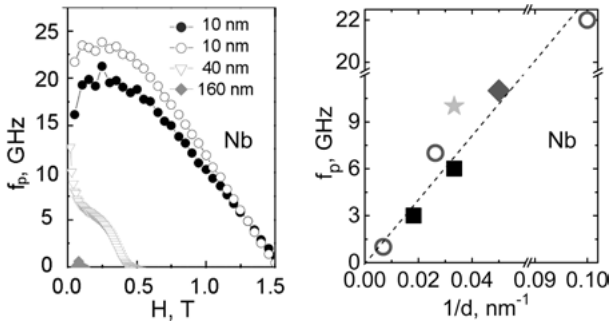

Fig. 8.2: Left: Dependence of f_p on the magnetic field value for a series of Nb films. Adapted with permission from [30]. Right: Film thickness dependence of f_p, extrapolated at $T = 0$, $H = 0$, for a series of Nb films: ★[32], ♦ [31], ○[30], ■ [33, 34]. Straight line is a guide for the eye.

properties represented by k_p. Thus, a unified model for the field and temperature dependences of f_p is quite unfeasible, and one has to rely on phenomenological or empirical laws. In general, f_p is a decreasing function of the temperature, with a weak temperature dependence not too close to T_c; f_p can often be approximated as $f_p(T) = f_p(0)[1 - (T/T_c)^4]$ [29]. As a function of H, the empiric expression $f_p(H) = f_p(0)[1 - (H/H_{c2})^2]$ [30] was found to fit the data. In addition, it appears that in thin films a thickness dependence arises in f_p: an extensive series of microwave experiments with Nb films [30–34] suggests that $f_p(H \to 0, T \to 0)$ follows the phenomenological law $f_p \propto 1/d$, where d is the film thickness. These dependences are presented in Figure 8.2.

The neglected thermal activation term corresponds to the flux-creep phenomena that are enhanced in High-Temperature Superconductors (HTSC) due to the high operating temperatures and small coherence volume. It is then mandatory to also consider the thermal activation. It has been shown that, despite the specific mechanism that is invoked to solve Equation (8.10), the result can be written in a generalized form as [5]:

$$\rho_v = \rho_{v1} + i\rho_{v2} = \frac{\Phi_0 B}{\eta} \frac{\chi + i\omega/\omega_0}{1 + i\omega/\omega_0} \tag{8.15}$$

where ρ_{v1} and ρ_{v2} are the real and imaginary part of the vortex-motion complex resistivity, and now flux creep enters via both the *creep factor* $\chi(T, H)$ and the new characteristic frequency, $\omega_0 \neq \omega_p$. The specific relations between the activation energy U, the creep factor χ, and ω_0 and ω_p depend on the model chosen for the treatment of the thermal effects. As an example, in the Brandt model (Equation (8.8)) one has $\omega_0 = \tau_p^{-1} + \tau_B^{-1}$, showing immediately that two characteristic times exist: the depinning time and the thermal vortex relaxation time. Figure 8.3 reports the frequency dependence of the calculated real and imaginary parts of ρ_v for finite creep. Comparison with the zero-creep limit (GR model, Equation (8.11)) reveals the main differences. First, the peak in ρ_2 is reduced by a factor $1-\chi$. Second, at low frequency $\rho_1 \neq 0$. About

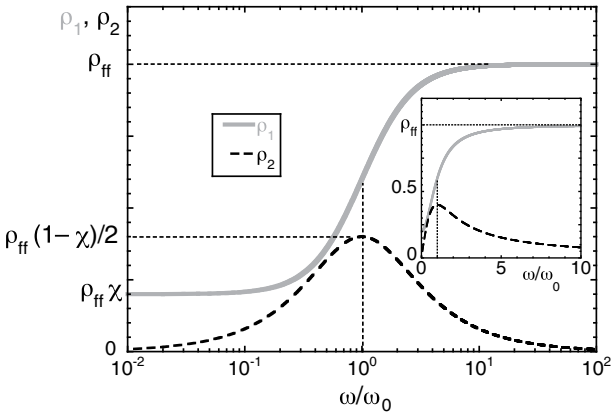

Fig. 8.3: Frequency dependence of the full vortex motion complex resistivity, for finite creep $\chi = 0.2$. At ω_0, ρ_1 reaches half of its maximum, and ρ_2 has the peak. Several relevant values are reported in the figure. Note that, because of creep effects, in the limit of zero frequency $\rho_1 \neq 0$. Inset: same as in the main panel, but replotted with linear abscissa.

the low-frequency limit, one should note that the model is likely to break down: at low frequencies the vortex displacement increases, the single-vortex approximation is no longer applicable and vortex-vortex effects become dominant. In fact, a low-frequency crossover toward vortex-glass dynamics has been observed in wideband (45 MHz–50 GHz) experiments in $YBa_2Cu_3O_{7-\delta}$ [35]. However, the high-frequency limit keeps the value ρ_{ff}, irrespective of thermally activated phenomena.

In experiments, one often relies on the microwave response measured at a single frequency. In this case, while Equation (8.11) can be inverted to directly obtain η and k_p (or f_p), Equation (8.15) contains the additional creep parameter χ and the problem is underconstrained. However, it is possible to exploit several mathematical and physical properties, in order to obtain useful estimates for the vortex parameters. It can be shown that, irrespective of the model adopted, in Equation (8.15) one always has [5]:

$$\chi < \chi_M = 1 + 2r^2 - 2r\sqrt{1 + r^2} \tag{8.16}$$

$$\eta_{GR}\frac{1 + \chi_M}{2} < \eta < \eta_{GR} \tag{8.17}$$

where η_{GR} is obtained through the GR model, and r is experimental (Equation (8.14)). Thus, it is always possible to have an estimate of the maximum value of the creep factor, χ_M, compatible with the data (upper limit for χ), and of the maximum uncertainty on η. A refined analysis in statistical terms shows that η obtained from the GR model is close to the most probable value. For what concerns k_p, the estimate of the uncertainty is model-dependent. In particular, within the Brandt model the GR estimate is again close to the real value. In any case, the data allow one to determine χ_M, and then it is possible to have a measure of the uncertainties on the vortex parameters. It

is clear that with multifrequency or swept-frequency measurements, one can directly apply Equation (8.15) and obtain all the vortex parameters.

8.3 High-frequency vortex dynamics in thin films

The response up to now described by Equations (8.11) or (8.15) takes into account a uniform current density $\boldsymbol{J}$, due to their origin as a single-vortex response. However, in real experiments it is important to ascertain the relation with the measured response function. We consider the general case of an e.m. field incident on a flat interface between a generic medium and a (super)conductor. The response is given by the *surface impedance* [36, 37] $Z_s = E_{||}/H_{||}$, where $E_{||}$ and $H_{||}$ are the tangential components of the electric and magnetic field, respectively. In the case of a bulk sample (thick with respect to the fields penetration depth) in the local limit, this quantity can be written in the two equivalent forms:

$$Z_s = \mathrm{i}\omega\mu_0\tilde{\lambda} = \sqrt{\mathrm{i}\omega\mu_0\rho} \tag{8.18}$$

where $\tilde{\lambda}$ is an appropriate complex screening length and the complex resistivity $\rho = \mathrm{i}\omega\mu_0\tilde{\lambda}^2$. The complex resistivity ρ (or equivalently $\tilde{\lambda}$ or Z_s) of a superconductor in the mixed state includes contributions from the moving vortex lattice, e.g., Equation (8.15), and from the superfluid and quasiparticle dynamics. A general treatment of the coupled dynamics in the linear response regime [20] yields:

$$\tilde{\lambda} = \left(\frac{\lambda^2 - (\mathrm{i}/2)\delta_\nu^2}{1 + 2\mathrm{i}\lambda^2/\delta_{\mathrm{nf}}^2}\right)^{1/2} \tag{8.19}$$

where, in addition to the usual London penetration depth λ, we defined the normal fluid skin depth $\delta_{\mathrm{nf}} = (2/\mu_0\omega\sigma_{\mathrm{nf}})^{1/2}$ and the vortex penetration depth defined as $\delta_\nu = (2\rho_{\mathrm{v}}/\mu_0\omega)^{1/2}$.

It is important to note that Equation (8.19) plays the role of a master equation, since various models can be invoked for the quantities λ, σ_{nf} and ρ_{v}, thus allowing it to be applied in very wide ranges of magnetic induction B, temperature T, and angular frequency ω.

While the combination of Equation (8.18) with Equations (8.19) and (8.15) may suggest that the number of parameters is exceedingly large with respect to the measurable quantities, it can be shown that in various circumstances the resulting expression is very tractable. We consider specifically the case of thin superconducting films. Let us consider a superconducting film, of thickness d, deposited onto a dielectric substrate. It has been shown [38, 39] that, when $d \lesssim \lambda, \delta$, the surface resistance takes the approximate form $Z_s = R_s + \mathrm{i}X_s \simeq \mathrm{i}\omega\mu_0\tilde{\lambda}^2/d$, reflecting the physical fact that the e.m. field

penetrates the sample almost uniformly.[6] In this case, since $\delta_{\rm nf} \gg \lambda$ apart very close to $T_{\rm c}$, and λ has a very weak dependence on the magnetic field, for the field variation of the surface impedance in thin films one has:

$$\Delta Z_s(H) = Z_s(H) - Z_s(0) = \Delta X + {\rm i}\Delta Y \simeq \frac{\rho_{\rm v}}{d} = \frac{\rho_{v1} + {\rm i}\rho_{v2}}{d} \tag{8.20}$$

Then, measurements in thin films are a very practical playground to directly obtain the vortex motion resistivity, and then the vortex parameters.

We finally mention that, by exploiting further the property $\delta_{\rm nf} \gg \lambda$, even in bulk samples (e.g., single crystals) one can show that the superfluid/quasiparticle and vortex motion contributions are approximately additive, and then $\Delta Z_s(H) \simeq \sqrt{{\rm i}\omega\mu_0\rho_{\rm v}}$. Although not as simple as Equation (8.20), this property allows one to extract the vortex parameters from measurements in bulk samples relatively easily [7].

8.4 Measurement techniques

In a typical setup, the superconducting sample is placed in some kind of device, connected to the external instrument with one or two ports. One measures in principle the forward $S_{21}(f)$ complex transmission coefficient, or the complex reflection coefficient $S_{11}(f)$, or both (Figure 8.4a). Changes in S_{ij} yield the changes in the properties of the device, and ultimately in the surface impedance of the superconductor under scrutiny. As a broad classification, the measurements can be performed with resonant or nonresonant systems.

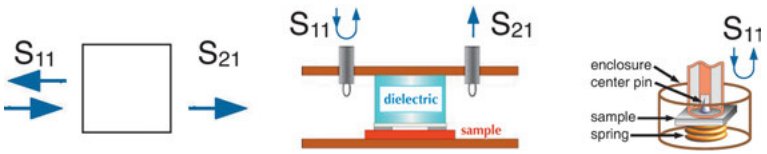

Fig. 8.4: (a) Sketch of a generic two-port device, containing the superconducting sample under investigation; (b) a typical dielectric resonator setup; (c) a typical Corbino disk setup.

Nonresonant methods are based on the measurements of the power reflected from, or transmitted through, the superconducting sample. Transmission-type measurements are not widely used in the microwave range due to low sensitivity and the need for complicated analytical modeling. Reflection-type measurements are more common. Previous nonresonant methods relied on the placement of a thin film sample in a

6 Substrate effects can appear when the substrate impedance attains particular values, and care must be taken in this case [40].

metallic waveguide, perpendicular to the axis of the waveguide. In this case the frequency span is limited by the waveguide cutoff, and is usually of a few GHz. In recent years, the wideband Corbino disk method has been developed following pioneering work at the University of Maryland [41]. The thin superconducting film terminates a coaxial cable, and the complex reflection coefficient $S_{11}(f, T, H)$ is measured (one-port measurement, Figure 8.4c). Despite a very complex and delicate calibration [42] and reduced sensitivity, the method can yield the microwave resistivity over one to three decades in frequency, and then it is a reliable method to directly assess the applicability of a relaxational dynamic class of models, represented by Equation (8.15) and Figure 8.3.

Resonant methods rely on either the perturbation of an external resonator, such as a metal cavity [43] or a dielectric resonator [44, 45] (Figure 8.4b), or on the patterning of a planar resonator on the superconductor. The surface impedance is related to the quality factor Q and the resonant frequency f_{res} of the device. Field changes in the resonator parameters yield the field changes of the surface impedance as:

$$\Delta Z(H) = G\left\{\left[\frac{1}{Q(H)} - \frac{1}{Q(0)}\right] - \mathrm{i}2\left[\frac{f_{\text{res}}(H) - f_{\text{res}}(0)}{f_{\text{res}}(0)}\right]\right\} \tag{8.21}$$

where G is a calculated geometrical factor. Note that in thin films (Equation (8.20)) one directly gets the vortex resistivity from the resonator parameters. Additional calibration is needed to obtain the absolute surface resistance. As a resonating technique, it has high inherent sensitivity, but is only single- or discrete-frequency.

Cavity/dielectric resonators are usually excited on the lowest order transverse electric TE or magnetic TM modes. When used in the surface perturbation technique (a planar superconducting sample replaces partially or entirely one of the walls of the resonator), they allow one to perform precise measurements of the surface impedance with sufficiently large samples. Small-sized samples in the form of platelets or single crystals can be studied by the volume-perturbation technique, where the sample is placed in the volume of the resonator.

Planar resonators such as microstrip [46] and coplanar [47] resonators are widely used for superconductor surface impedance measurements in the presence of a magnetic field and for the study of nonlinear effects due to the high microwave currents (that is, ac magnetic fields) that can be reached in the sample. Since the resonator is directly patterned on the superconducting film, this is a destructive technique. They present quite large Q factors, of the order 10^4, which allow one to perform accurate measurements. However, a possible issue in the interpretation of the data comes from the fact that the effects of the sample boundaries play a role in the overall Q, and less-than-perfect lithography may severely affect the overall response.

In some cases, the resonator is simply tuned at the resonant frequency, and only the power reflected (or transmitted) at the resonance is measured. This simpler technique gives no access to the imaginary part of the resistivity or surface impedance, but may prove effective for measurements of the surface resistance (real part of the

response). As an example, the measurements in Figure 8.1 were obtained in this fashion.

A related quantity which can be probed in microwave measurements with a two-port device is the forward transmission coefficient $S_{21}(f)$. Its absolute value is a measure of the ratio of microwave power at port 2 to that at port 1 and, hence, it allows one to directly access the insertion loss at microwave frequencies in the superconductor under study. This type of broadband microwave measurement will be exemplified in Section 8.7.

8.5 Microwave vortex response in S/F/S heterostructures

We begin our series of examples of the microwave response of vortices in nanostructured superconductors by considering the progressive change in the vortex parameters in superconductor/ferromagnet/superconductor (S/F/S) heterostructures with increasing thickness of the ferromagnetic layer. Such heterostructures are of prominent fundamental interest for the competition between superconducting and ferromagnetic ordering (Chapters 13, 15), but applications can be envisaged (Chapter 14). In this example, we are interested mainly in an illustration of the broad features that can be observed by the study of the vortex dynamics at microwave frequencies. We consider heterostructures with an F layer (in our case, a Pd and Ni alloy of nominal composition $Pd_{0.84}Ni_{0.16}$) of thickness $d_F = 1, 2, 8, 9$ nm, sandwiched between two superconducting Nb layers of nominal thickness $d_S = 15$ nm [48, 49]. Pure Nb samples of total thickness $d = 20$ nm and 30 nm serve as references. Measurements were performed by both the Corbino disk and dielectric resonator (8 GHz) techniques. Figure 8.5 reports typical Corbino disk measurements in different samples, and some of the relevant vortex parameters. In this case, we discuss the flux-flow regime in terms of the flux-flow resistivity ρ_{ff}, since it is a directly obtained parameter, see Equation (8.15), and it can also be evaluated by simple inspection of the $\rho_{v1}(f)$, since it is the asymptotic plateau.

Figure 8.5a–c reports some sample curves for $\rho_{v1}(f)$ [31]. An important message comes from the raw data: the relaxational dynamics (Equation (8.15)) holds in these systems, so it is meaningful to proceed further in the analysis of the data. This is not trivial, in particular when an exotic system like S/F/S is scrutinized. Continuous lines represent fits with ρ_{v1} from Equation (8.15); from the fits, one obtains the normalized ρ_{ff}/ρ_n, the creep factor χ, and the characteristic frequency $\omega_0/2\pi$. Figure 8.5d reports the flux-flow resistivity in the sample with $d_F = 1$ nm, at $T = 3.58$ K and as a function of the field (each data point is the result of a frequency sweep, and a fit of the obtained $\rho_{v1}(f)$). It is immediately seen that the simple BS expression, Equation (8.12) (dashed line), is not a satisfactory description of the data. Then, one must resort to more sophisticated theories. Within the time-dependent Ginzburg–Landau framework, the flux-flow resistivity has been calculated in the entire field range up to H_{c2}. The expression

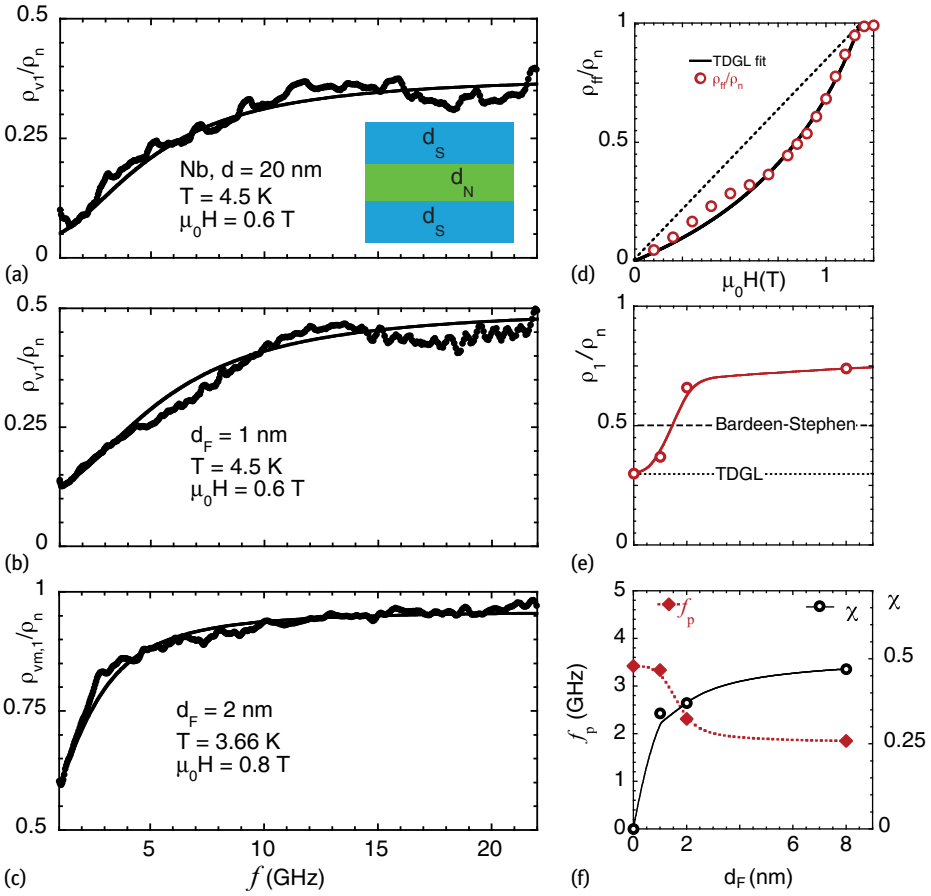

Fig. 8.5: (a)–(c) Corbino disk measurements $\rho_{v1}(f)/\rho_n$ in different S/F/S heterostructures. H is applied perpendicular to the F and S layers. Inset: sketch of the heterostructure and orientation of the magnetic field; continuous lines are fits with Equation (8.15). (d) Normalized flux-flow resistivity ρ_{ff}/ρ_n as a function of the applied field at fixed temperature, in the sample with $d_F = 1$ (open circles); continuous line: TDGL theory with $\alpha = 0.4$, dashed line: Bardeen–Stephen expression, $\rho_{ff} = \Phi_0 B/\eta$, with field-independent η. (e) d_F dependence of the normalized plateau resistivity, $\rho_{plateau} \sim \rho_{ff}$ [50], and the expected values for the Bardeen–Stephen model, Equation (8.12), and the TDGL theory, Equation (8.22). Flux-flow resistivity in excess of the Bardeen–Stephen model is clearly observed as a consequence of increasing d_F. The red continuous line is a guide to the eye. $d_F = 0$ represents a Nb sample, 30 nm thick. (f) d_F dependence of the depinning frequency, f_p (red diamonds), and of the creep factor χ (open circles), from [32]. Lines are guides to the eye. Since both quantities depend upon the London penetration depth, this is a clear indication that λ increases with d_F (see text).

reads [51]:

$$\rho_{\mathrm{ff}} = \rho_{\mathrm{n}} \frac{1}{1 + (\mu_0 H_{\mathrm{c2}} - B)/\alpha B} \tag{8.22}$$

where $\alpha \approx 0.4$ has been calculated in [52] (the BS model is recovered with $\alpha = 1$). This model (continuous line in Figure 8.5d) nicely fits the data. However, additional phenomena arise in the flux-flow resistivity with increasing d_{F}. In Figure 8.5e we report the plateau resistivity of the normalized curves $\rho_{\mathrm{v1}}(f)/\rho_{\mathrm{n}}$, that is an experimental measure of ρ_{ff}, as a function of d_{F} and at the same reduced temperature $T/T_c \simeq 0.86$ and reduced field $H/H_{\mathrm{c2}} \simeq 0.5$ [50]. It is immediately seen that, when the effect of the ferromagnetic layer becomes appreciable, the flux-flow resistivity increases and exceeds the Bardeen–Stephen value. This is an intriguing result: keeping in mind that, as an approximate relation, $\rho_{\mathrm{ff}} \sim 1/n_{\mathrm{qp}}, 1/\tau_{\mathrm{qp}}$, this is a clear indication that the increase of the thickness of the F layer brings a shortening of the quasiparticle lifetime, or a reduction of their concentration, or both.

Turning the attention to the pinning properties, we report in Figure 8.5f the creep factor χ, and the depinning frequency f_{p} (derived from ω_0 and χ) as a function of d_{F} [32]. The increase of the ferromagnetic thickness d_{F} determines an increase of the creep factor, and a decrease of the depinning frequency. In fact, both quantities are related to the condensation energy. In particular, for core pinning, one can estimate [11] $\frac{1}{2} k_{\mathrm{p}} \xi^2 \approx c_{\mathrm{p}} \frac{1}{2} \mu_0 H_{\mathrm{c}}^2 \xi^2$ ($c_{\mathrm{p}} \sim 1$). Recalling that $H_{\mathrm{c}}^2 \approx H_{\mathrm{c1}} H_{\mathrm{c2}}$, and $H_{\mathrm{c1}} \simeq \Phi_0/4\pi\lambda^2$, and making use of the BS expression for η as a very crude approximation, in this very simplified model one has $f_{\mathrm{p}} \propto \lambda^{-2}$. Thus, the measurements of the vortex motion here presented are an indication that the ferromagnetic layer is responsible for the increase of the London penetration depth or, which is the same, for the decrease of the superfluid.

Thus, measurements of the vortex response under microwave fields can give information on both the underlying superfluid and quasiparticle states, and their changes with nanosize geometrical changes such as the thickness of the F layer in S/F/S heterostructures.

8.6 Microwave vortex response in $YBa_2Cu_3O_{7-\delta}$ with nanorods

The study of the microwave vortex response is a powerful tool also in connection to the optimization of materials for power applications. In this field, it is now assessed that second-phase nanoprecipitates determine very strong pinning centers (Chapter 3). Interestingly, in thin $YBa_2Cu_3O_{7-\delta}$ films grown by Pulsed Laser Deposition, $BaZrO_3$ second phases often self-assemble in the shape of elongated defects, threading entirely or partially the thin film approximately parallel to the c-axis, producing so-called " nanorods" due to their diameter of a few nm. This peculiar shape makes such nanorods very similar, in their effects, to columnar defects, and they produce a large increase of the in-field critical current density, and of the volume pinning force.

Since, as has been described above, microwaves are capable of simultaneously investigating both pinning and quasiparticle states, such $YBa_2Cu_3O_{7-\delta}/BaZrO_3$ systems are certainly of interest as illustrative examples of nanoengineered superconductors of applicative significance.

The example that we illustrate here is taken from measurements of the microwave complex resistivity by means of the dielectric resonator technique at the very high operating frequency $f \sim 47$ GHz. We concentrate on a series of samples with different molar concentration of $BaZrO_3$: 0, 2.5, 5, and 7% [53]. In Figure 8.6a–e we show sample measurements of the thin film vortex surface impedance $\rho_v(H)/d$ in a sample of $YBa_2Cu_3O_{7-\delta}/BaZrO_3$ at 5% mol at $T = 80$ K, illustrating the different vortex parameters as they can be extracted using the constraints described in Section 8.2. Panel (a) reports the raw data for $\rho_v(H)/d$ as a function of the applied field, along the c-axis. Panel (b) reports the field dependence of r (Equation (8.14)), and panel (c) reports the field dependence of the maximum creep factor (the upper limit) χ_M (Equation (8.16)). We recall that r is a proxy for $f_p \simeq rf$, where $f \simeq 47.5$ GHz is the measuring frequency. Then, the results of Figure 8.6b indicate that the addition of nanorods has increased the depinning frequency up to the very high value $f_p \simeq 65$ GHz at low fields, as opposed to reported values in the range $\sim$ 10–20 GHz [11]. Consistently, panel (c) shows that the creep factor never exceeds 0.1, so that creep is a relatively unlikely phenomenon even at the high $T = 80$ K of these measurements. Panel (d) reports the flux-flow resistivity as derived from the data in (a). Here, it is instructive to report the maximum information that can be gained from the data. Using the procedure depicted in Section 8.2, and extensively discussed in [5], we plot the GR value (thick black line), the maximum ρ_{ff} compatible with the data, originating from Equation (8.17) (thin black line), the interval where we expect to find ρ_{ff} with 90% probability (shaded area), and finally the expected value $\langle\rho_{ff}\rangle$, red open symbols. From this discussion, it is reassuring that the GR estimate is a very good approximation of the expected value for ρ_{ff}. Panel (e) reports the derived pinning constant k_p; the discussion is analogous to the discussion of ρ_{ff}, with the additional remark that a specific model needs to be adopted to derive the uncertainty-related values. In this case, we have adopted the Brandt model.

Thus, the addition of nanorods increases significantly the pinning strength, and this effect is visible at microwave frequencies: this is not trivial, because microwaves probe the very short-range dynamics (very small vortex oscillations), so these results imply that not only is the pinning potential induced by the nanorods deep (small χ_M), but also that it is very steep (large k_p, the elastic recall constant). It is then interesting to study the dependence of the various vortex parameters with the $BaZrO_3$ concentration. This is exemplified in Panels (f)–(h), where it is shown that the pinning-related parameters, r and k_p, increase significantly with $BaZrO_3$ [54, 55]. We mention that also η changes, although by a smaller factor. This may suggest that the nanorods have some effect on the quasiparticle properties.

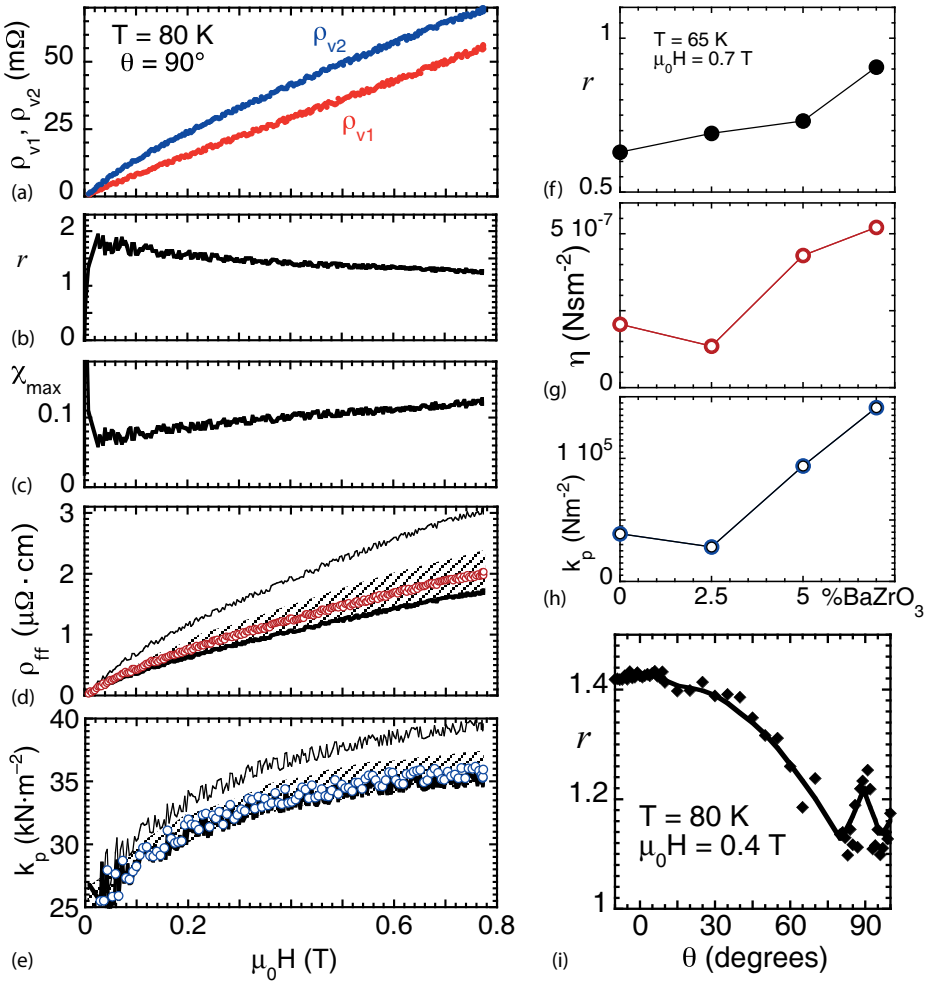

Fig. 8.6: (a)–(e) Vortex motion complex resistivity versus the applied field in a $YBa_2Cu_3O_{7-\delta}/BaZrO_3$ sample at 80 K, with the field along the *c*-axis. (a) Raw data. (b) *r* Parameter; since the measuring frequency is $f = 47.5$ GHz, $r \simeq f_p/f > 1$ indicates a very strong pinning. (c) Maximum creep factor (upper limit). (d) Flux-flow resistivity and refined analysis: thick black line, GR estimate; thin black line, maximum value compatible with the data; shaded gray band: 90% confidence band [5]; red empty symbols: average value. As can be seen, the GR value is a good measure when creep is small. (e) Pinning constant k_p. Black symbols and shaded area, same meaning as in (d), blue empty symbols: average values. Again, the GR estimate is a good measure. (f)–(h) Dependence of the vortex parameters with the $BaZrO_3$ concentration, showing increasing pinning with $BaZrO_3$, and a possible dependence of η. (i) Demonstration of the directional pinning of $BaZrO_3$ nanorods: the angle θ between *H* and the *c*-axis is varied: the *r* parameter, a proxy for f_p, is larger along the nanorods ($\theta = 0$) than when the field is along the CuO planes.

Finally, we demonstrate the strong directionality of the nanorods-induced vortex pinning. Measurements of the vortex resistivity were taken at fixed field and temperature, by varying the angle θ with the c-axis, where the nanorods align. In pinning-free, ideal $YBa_2Cu_3O_{7-\delta}$ we expect an increase of the pinning strength (e.g., the r parameter or f_p) approaching $\theta = 90°$ [11], where intrinsic pinning by the ab-planes is effective. The measurements of r reported in Figure 8.6i do indeed show a peak at this angle, but the peak is taken over by a broad, higher peak in r with $\theta = 0°$, that is with the field aligned with the nanorods [4, 56]. Following the above discussion of k_p, the present microwave measurements show evidence that the $BaZrO_3$ nanorods induce very deep and steep pinning wells along the nanorods themselves.

Summarizing the last two Sections, we have shown by using examples how the microwave investigation can unveil a full variety of phenomena in the vortex motion in nanostructured superconductors. We will conclude this short survey by presenting the behavior of the vortex matter when subjected to a dc current superimposed to the microwave field.

8.7 Microwave vortex response in Nb films with nanogroove arrays

The depinning frequency f_p can be tuned not only by the thermodynamic quantities T and H, but also by the experimental parameters such as the pinning strength and the dc current density J. Namely, the fabrication of periodic pinning sites in superconductors allows one to increase f_p, whereas f_p can be reduced by superimposing a dc bias onto the microwave stimulus. Already the first experiments on the microwave power absorbed by vortices revealed that the depinning frequency f_p is higher in superconductors with strong pinning [25]. Accordingly, microwave losses due to motion of vortices can be minimized by confining them by strategically positioned pinning sites, see also Chapter 7. In residual ambient fields, energy losses in superconducting planar resonators due to a small number of vortices, caught while cooling through the superconducting transition, can be reduced by trapping them within a slot patterned into the resonator [46]. For larger fields, antidots fabricated along the conductors' edges allow one to increase the quality factor of niobium stripline resonators [57]. For circuit elements with a width greater than 100 μm, patterning of the entire surface of the superconductor with periodic arrays of pinning sites turned out to be most efficient [33, 34, 58–61], see Figure 8.7a for the typical geometry.

At the same time, the effective pinning intensity can be reduced under the action of a dc bias superimposed onto the microwave stimulus [63, 64]. When the vortex lattice geometrically matches the periodic pinning landscape, the vortex-vortex interaction is effectively canceled [65], the microwave power absorbed by vortices exhibits a minimum [33, 60, 61], and the dynamics of the entire vortex ensemble can be re-

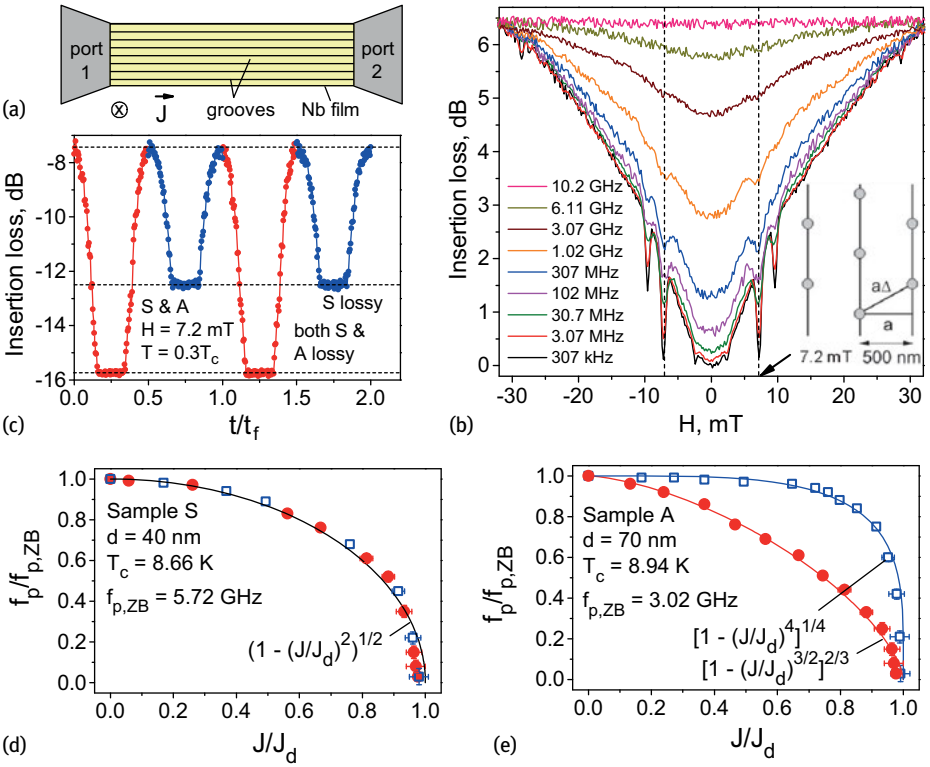

Fig. 8.7: (a) Experimental geometry [62]: Samples S and A are 40 nm- and 70 nm-thick $150\times500\ \mu m^2$ Nb microstrips with nanogroove arrays. The zero-bias depinning frequencies of samples S and A, $f_{p,ZB} = f_p(J_{dc} = 0)$, amount to $f_{p,ZB} = 5.72$ GHz and $f_{p,ZB} = 3.02$ GHz, respectively. (b) Insertion losses due to vortices in sample A under magnetic field reversal [33]. (c) Tailoring discrete insertion loss levels [34] by a serial connection of samples S and A for an ac frequency 3.02 GHz and an ac amplitude $I = 50$ mA corresponding to $J = 0.48\ MA/cm^2 \simeq J_d^+ = 0.52\ MA/cm^2$ for sample A and $J = 0.83\ MA/cm^2 \simeq J_d = 0.75\ MA/cm^2$ for sample S, see also Figure 8.8. The time t is in units of the period of the quasistatic ac current with $1/t_f = 3$ Hz. (d), (e) Reduction of the depinning frequency upon increasing the dc density as deduced from the microwave power absorption data [33]. The experimental data for the positive (•) and the negative (□) dc polarity are approximated by fits (solid lines) of the general form $f_p(J)/f_{p,ZB} = [1 - (J/J_d)^{k/l}]^{m/n}$, with the exponents k, l, m, n as indicated. The data in panels (c–e) are acquired at the fundamental matching field $H = 7.2$ mT at $T \approx 0.3T_c$. The red and blue curves (symbols) in panels (c)–(e) correspond to the positive and negative dc polarity, respectively. Reproduced with permission from [33, 34].

garded as that of the single average vortex in the average pinning potential. This is exemplified in Figure 8.7b where the microwave insertion loss is at a minimum for the lattice parameter $a_\triangle = (2\Phi_0/H\sqrt{3})^{1/2}$ and the matching condition $a_\triangle = 2a/\sqrt{3}$ in a washboard nanolandscape with period $a = 500$ nm at the fundamental matching field $H = 7.2$ mT, as sketched in the inset. In particular, this validates single-vortex

models [5, 20, 22–25, 64, 66, 67] for analyzing the vortex dynamics at microwave frequencies.

A coherent vortex dynamic leads to the appearance of quantum interference effects (Shapiro steps) in the current-voltage curves (CVC) of the samples, each time one or a multiple of the hopping distance of the vortex rows during one half ac cycle coincides with the nanostructure period [68]. Shapiro steps were first observed in the CVC of microwave-excited Josephson junctions [69], as considered in Chapters 10, 11, and 12, and they were extensively studied in superconductors with a moving vortex lattice [68, 70–76]. Shapiro steps are inherent to the force-velocity characteristics of systems described in terms of a particle moving in a periodic potential under combined dc and ac stimuli [77–80]. Because of the coherent motion of Abrikosov vortices further effects emerge in the vortex dynamics under combined dc and microwave drives [33, 34], some of which are outlined next.

The reduction of the depinning frequency upon increasing the dc value can be understood as a consequence of the effective lowering of the pinning potential well due to its tilt by the dc bias, as exemplified for two nanopatterned Nb films S and A in Figure 8.7d and e. This scenario is most visual for a washboard pinning potential, whose symmetric (S) and asymmetric (A) representatives are shown in the insets to Figure 8.8a and b, respectively. The simple form of these potentials allows for an exact analytical description [22–24] of the resistive response and the absorbed microwave power in superconductors as functions of the driven parameters, thus providing the basis for Abrikosov fluxonics in washboard nanolandscapes [81]. Namely, the mechanistic consideration [22–24] of a vortex as a particle suggests that during an ac semiperiod, while the pinning potential well is broadening due to its tilt under the action of the dc bias, with increasing frequency f the vortex no longer has time ($\sim 1/f$) to reach the areas where the pinning forces dominate and, hence, the dissipative response is stronger already at lower frequencies compared to the zero-bias case. The same mechanistic scenario can explain the difference in the reduction of the depinning frequencies for the positive and the negative dc biases in Figure 8.7e, caused by the different groove slope steepnesses in sample A [24]. This is reinforced by the study of the dc depinning current density, J_d, on the same samples. In fact, the groove asymmetry causes a difference in the depinning current densities J_d^+ and J_d^- for the positive and negative branches of the CVC for sample A in Figure 8.8b. This is in contrast to the CVC of sample S where $J_\mathrm{d}^+ = J_\mathrm{d}^- \equiv J_\mathrm{d}$, Figure 8.8a. Therefore, while both samples exhibit a microwave cut-off filter behavior [33], the cut-off frequency of sample A, which is determined by f_p, can be tuned not only by the dc value but also by its polarity. At microwave frequencies this effect is complementary to the low-frequency vortex ratchet effect [82] introduced in Chapter 7.

The dependence of the depinning frequency on the nanopattern type and the dc bias value allows one to use superconducting planar transmission lines with different nanopatterns for tailoring discrete microwave loss levels [34]. When one applies a quasistatic ac current $I \equiv I(t) = I \sin \omega t$ with $f \equiv 1/t_f = 3$ Hz, $\omega = 2\pi f$, to samples S

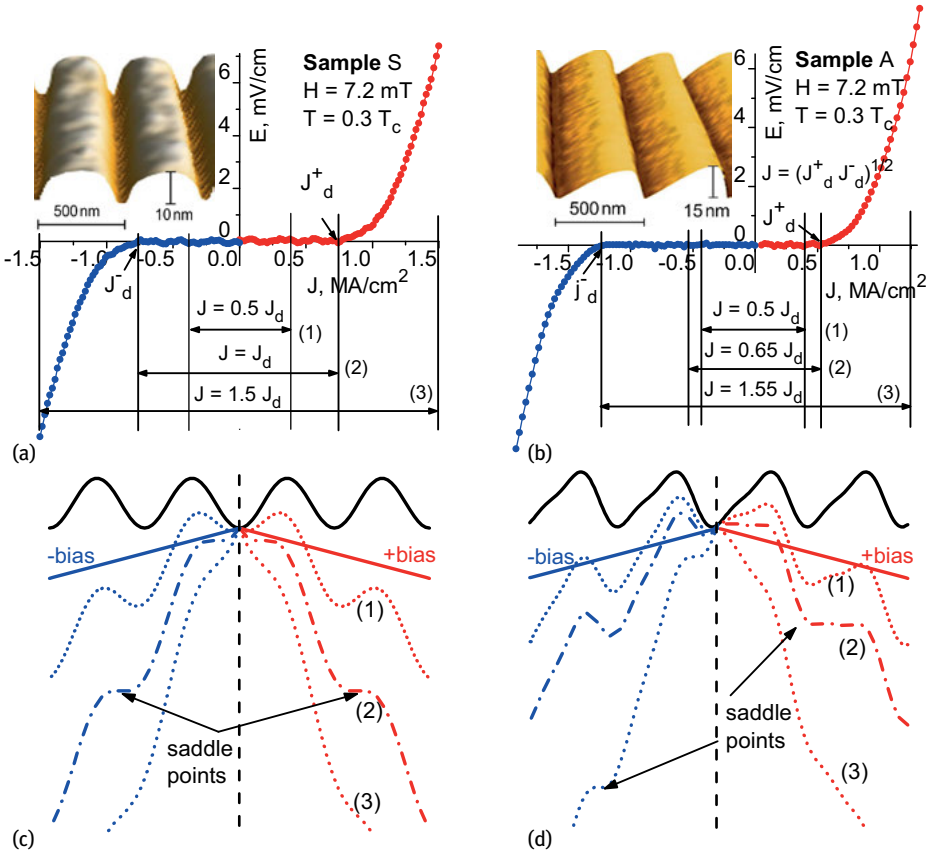

Fig. 8.8: (a), (b) CVCs of Nb films S and A with the quasistatic ac amplitudes corresponding to the different dynamic regimes shown by the horizontal arrows. (c), (d) Tilts of the washboard potentials sketched for the ac amplitudes (1)–(3) in the CVCs corresponding to panels (a) and (b), respectively. The left and right halves of panels (c) and (d) correspond to the negative and positive current polarity, respectively. Reproduced with permission from [34].

and A connected in series, a sine-to-triangular and a sine-to-rectangular pulse shape conversion [34] is observed depending upon which of operating regimes (1), (2), and (3) is chosen in their CVC, refer to Figure 8.8. These regimes correspond to the cases when the vortex is shaken within one and the same well (1), when the vortex runs on the tilted washboard (3), and the nonlinear transient regime (2) when one of the barriers vanishes. For definiteness, when the ac amplitude is chosen so that regime (2) is realized for each of samples S and A connected in series, the cumulative insertion loss in Figure 8.7c is characterized by three different levels, whereby the intermediate level is achieved in consequence of the combination of the lossy state of microstrip S and the low-lossy state of microstrip A. Therefore, the combination of differently pat-

terned superconducting transmission lines allows one to use them as building blocks for fluxonic metamaterial with discrete insertion loss levels.

8.8 Conclusion

The study of the vortex dynamics at microwave frequencies is an interesting research subject hosting a rich fundamental physics and promising perspectives for superconducting microwave applications. Because of the relatively high frequency range, it is possible to measure several important vortex parameters in the linear regime, such as the flux-flow resistivity (or vortex viscosity), the pinning constant, the depinning frequency, and the creep factor. This powerful technique proves to be particularly useful when one investigates the effects of artificial nanostructuring of superconductors, since the different behaviors induced by the nanostructure emerges clearly when compared to pristine or plain samples. The superposition of a dc and ac current allows one to dynamically tailor the response of nanostructured materials, and in perspective to develop dynamically tunable devices for operation in the microwave range.

8.9 Acknowledgements

We acknowledge useful discussions with C. Attanasio, A. Buzdin, G. Celentano, M. Huth, S. Sarti, V. A. Shklovskij, and K. Torokhtii. ES and NP acknowledge partial support by a PRIN project (SFS) and by EUROFUSION (for work in $YBa_2Cu_3O_{7-\delta}/BaZrO_3$). OD acknowledges support from the German Research Foundation (DFG) under Grant DO 1511 and the Goethe University funding program "Nachwuchswissenschaftler im Fokus". This work was conducted within the framework of the COST Action MP1201 of the European Cooperation in Science and Technology.

Bibliography

[1] Tinkham M. Introduction to Superconductivity. Mineola, New York, 2004.
[2] Embon L, Anahory Y, Suhov A, Halbertal D, Cuppens J, Yakovenko A, Uri A, Myasoedov Y, Rappaport ML, Huber ME, Gurevich A, Zeldov E. Probing dynamics and pinning of single vortices in superconductors at nanometer scales Sci Rep. 5:7598, 2015.
[3] Pompeo N. Analysis of pinning in the linear ac response of anisotropic superconductors in oblique magnetic fields J. Appl. Phys. 117:103904, 2015.
[4] Pompeo N, Augieri A, Torokhtii K, Galluzzi V, Celentano G, Silva E. Anisotropy and directional pinning in $YBa_2Cu_3O_{7-x}$ with $BaZrO_3$ nanorods Appl. Phys. Lett. 103:022603, 2013.
[5] Pompeo N, Silva E. Reliable determination of vortex parameters from measurements of the microwave complex resistivity Phys. Rev. B 78:094503, 2008.

[6] Bardeen J, Stephen MJ. Theory of the motion of vortices in superconductors Phys. Rev. 140:A1197–A1207, 1965.
[7] Tsuchiya Y, Iwaya K, Kinoshita K, Hanaguri T, Kitano H, Maeda A, Shibata K, Nishizaki T, Kobayashi N. Electronic state of vortices in YBa2Cu3Oy investigated by complex surface impedance measurements Phys. Rev. B 63:184517-1–184517-9, 2001.
[8] Zhou XQ, Truncik C J S, Huttema WA, Murphy NC, Turner PJ, Koenig AJ, Liang RX, Bonn DA, Hardy WN, Broun DM. Microwave spectroscopy of vortex dynamics in ortho-II $YBa_2Cu_3O_{6.52}$ Phys. Rev. B 87:184512, 2013.
[9] Caroli C, Gennes PD, Matricon J. Bound fermion states on a vortex line in a type II superconductor Phys. Lett. 9:307–309, 1964.
[10] Blatter G, Feigel'man MV, Geshkenbein VB, Larkin AI, Vinokur VM. Vortices in high-temperature superconductors Rev. Mod. Phys. 66:1125–1388, 1994.
[11] Golosovsky M, Tsindlekht M, Davidov D. High-frequency vortex dynamics in YBa2Cu3O7 Supercond. Sci. Technol. 9:1–15, 1996.
[12] Kopnin NB. Vortex dynamics and mutual friction in superconductors and Fermi superfluids Rep. Progr. Phys. 65:1633, 2002.
[13] Kopnin NB, Volovik GE. Flux Flow in d-Wave Superconductors: Low Temperature Universality and Scaling Phys. Rev. Lett. 79:1377–1380, 1997.
[14] Kopnin NB. Resonant absorption at the vortex-core states in d-wave superconductors Phys. Rev. B 57:11775–11785, 1998.
[15] Yeh NC. High-frequency vortex dynamics and dissipation of high-temperature superconductors Phys. Rev. B 43:523–531, 1991.
[16] Hsu TC. Absence of dipole transitions in vortices of type-ii superconductors Phys. Rev. B 46:3680–3683, 1992.
[17] Choi EJ, Lihn H T S, Drew HD, Hsu TC. Magneto-optics of type-II superconductors Phys. Rev. B 49:13271–13274, 1994.
[18] Miller D, Richards PL, Merchant P. Magnetic-field effects on submillimeter absorptivity in epitaxial thin films of $YBa_2Cu_3O_7$ Phys. Rev. B 51:8385–8389, 1995.
[19] Tomasch WJ, Blackstead HA, Ruggiero ST, McGinn PJ, Clem JR, Shen K, Weber JW, Boyne D. Magnetic field dependence of nonresonant microwave power dissipation in $YBa_2Cu_3O_{7-x}$ Phys. Rev. B 37:9864–9867, 1988.
[20] Coffey MW, Clem JR. Unified theory of effects of vortex pinning and flux creep upon the rf surface impedance of type-II superconductors Phys. Rev. Lett. 67:386–389, 1991.
[21] Brandt EH. Penetration of magnetic ac fields into type-ii superconductors Phys. Rev. Lett. 67:2219–2222, 1991.
[22] Shklovskij VA, Dobrovolskiy OV. AC-driven vortices and the Hall effect in a superconductor with a tilted washboard pinning potential Phys. Rev. B 78:104526, 2008.
[23] Shklovskij VA, Dobrovolskiy OV. Frequency-dependent ratchet effect in superconducting films with a tilted washboard pinning potential Phys. Rev. B 84:054515, 2011.
[24] Shklovskij VA, Sosedkin VV, Dobrovolskiy OV. Vortex ratchet reversal in an asymmetric washboard pinning potential subject to combined dc and ac stimuli J. Phys.: Cond. Matt. 26:025703, 2014.
[25] Gittleman JI, Rosenblum B. Radio-frequency resistance in the mixed state for subcritical currents Phys. Rev. Lett. 16:734–736, 1966.
[26] Campbell AM, Evetts JE. Flux vortices and transport currents in type II superconductors Adv. Phys. 21:199–428, 1972.
[27] Halbritter J. rf residual losses, surface impedance, and granularity in superconducting cuprates J. Phys. III 68:6315–6326, 1990.

[28] Halbritter J. Transport in superconducting niobium films for radio frequency applications J. Appl. Phys. 97:083904-1–083904-12, 2005.
[29] Zaitsev AG, Schneider R, Linker G, Ratzel F, Smithey R, Geerk J. Effect of flux flow on microwave losses in $YB_2Cu_3O_{7-x}$ superconducting films Phys. Rev. B 68:104502, 2003.
[30] Janjušević D, Grbić MS, Požek M, Dulčić A, Paar D, Nebendahl B, Wagner T. Microwave response of thin niobium films under perpendicular static magnetic fields Phys. Rev. B 74:104501, 2006.
[31] Silva E, Pompeo N, Sarti S. Wideband microwave measurements in Nb/Pd84Ni16/Nb structures and comparison with thin Nb films Supercond. Sci. Technol. 24:024018, 2011.
[32] Pompeo N, Torokhtii K, Meneghini C, Mobilio S, Loria R, Cirillo C, Ilyina E, Attanasio C, Sarti S, Silva E. Superconducting and structural properties of Nb/PdNi/Nb trilayers J. Supercond. Nov. Magnet. 26:1939–1943, 2013.
[33] Dobrovolskiy OV, Huth M. Dual cut-off direct current-tunable microwave low-pass filter on superconducting Nb microstrips with asymmetric nanogrooves Appl. Phys. Lett. 106:142601, 2015.
[34] Dobrovolskiy OV, Huth M, Shklovskij VA. Alternating current-driven microwave loss modulation in a fluxonic metamaterial Appl. Phys. Lett. 107:162603, 2015.
[35] Wu DH, Booth J, Anlage S. Frequency and field variation of vortex dynamics in YBa2Cu3O7-d Phys. Rev. Lett. 75:525–528, 1995.
[36] Jackson JD. Classical Electrodynamics. Wiley, 1962.
[37] Collin RE. Foundation for Microwave Engineering. McGraw-Hill International Editions, 1992.
[38] Sridhar S. Microwave response of thin-film superconductors J. Appl. Phys. 63:159–166, 1988.
[39] Silva E, Lanucara M, Marcon R. The effective surface resistance of superconductor/dielectric/metal structures Supercond. Sci. Technol. 9:934, 1996.
[40] Pompeo N, Muzzi L, Galluzzi V, Marcon R, Silva E. Measurements and removal of substrate effects on the microwave surface impedance of YBCO films on SrTiO3 Supercond. Sci. Technol. 20:1002, 2007.
[41] Booth JC, Wu DH, Anlage SM. A broadband method for the measurement of the surface impedance of thin films at microwave frequencies Rev. Sci. Instr. 65:2082–2090, 1994.
[42] Silva E, Pompeo N, Torokhtii K, Sarti S. Wideband surface impedance measurements in superconducting films IEEE Trans. Instrument. Meas. 65:1120–1129, 2016.
[43] Portis AM, Cooke DW, Gray ER. Rf properties of high-temperature superconductors: Cavity methods J. Supercond. 3:297–304, 1990.
[44] Krupka J, Klinger M, Kuhn M, Baryanyak A, Stiller M, Hinken J, Modelski J. Surface resistance measurements of hts films by means of sapphire dielectric resonators IEEE Trans. Appl. Supercond. 3:3043–3048, 1993.
[45] Pompeo N, Torokhtii K, Silva E. Dielectric resonators for the measurements of the surface impedance of superconducting films Meas. Sci. Rev. 14:164–170, 2014.
[46] Song C, DeFeo MP, Yu K, Plourde BLT. Reducing microwave loss in superconducting resonators due to trapped vortices Appl. Phys. Lett. 95:232501, 2009.
[47] Porch A, Lancaster MJ, Humphreys RG. The coplanar resonator technique for determining the surface impedance of YBa2Cu3O7-δ thin films IEEE Trans. Microwave Theor. Techn. 43:306–314, 1995.
[48] Pompeo N, Torokhtii K, Cirillo C, Samokhvalov AV, Ilyina EA, Attanasio C, Buzdin AI, Silva E. Thermodynamic nature of the $0 - \pi$ quantum transition in superconductor/ferromagnet/superconductor trilayers Phys. Rev. B 90:064510, 2014.
[49] Loria R, Meneghini C, Torokhtii K, Tortora L, Pompeo N, Cirillo C, Attanasio C, Silva E. Robustness of the $0 - \pi$ transition against compositional and structural ageing in superconductor/ferromagnetic/superconductor heterostructures Phys. Rev. B 92:184106, 2015.

[50] Torokhtii K, Pompeo N, Meneghini C, Attanasio C, Cirillo C, Ilyina E, Sarti S, Silva E. Microwave properties of Nb/PdNi/Nb trilayers J. Supercond. Nov. Magnet. 26:571–574, 2013.
[51] Troy RJ, Dorsey AT. Transport properties and fluctuations in type-II superconductors near H_{c2} Phys. Rev. B 47:2715–2724, 1993.
[52] Liang M, Kunchur MN, Hua J, Xiao Z. Evaluating free flux flow in low-pinning molybdenum-germanium superconducting films Phys. Rev. B 82:064502-1–064502-5, 2010.
[53] Pompeo N, Rogai R, Silva E, Augieri A, Galluzzi V, Celentano G. Strong reduction of field-dependent microwave surface resistance in YBa2Cu3O7-δ with submicrometric BaZrO3 inclusions Appl. Phys. Lett. 91:182507, 2007.
[54] Pompeo N, Rogai R, Augieri A, Galluzzi V, Celentano G, Silva E. Reduction in the field-dependent microwave surface resistance in $YBa_2Cu_3O_{7-\delta}$ with submicrometric $BaZrO_3$ inclusions as a function of $BaZrO_3$ concentration J. Appl. Phys. 105:013927, 2009.
[55] Pompeo N, Rogai R, Galluzzi V, Augieri A, Celentano G, Ciontea L, Petrisor T, Silva E. Effect of $BaZrO_3$ inclusions on the microwave surface impedance of YBCO films in a magnetic field IEEE Trans. Appl. Supercond. 19:2917–2920, 2009.
[56] Pompeo N, Torokhtii K, Augieri A, Celentano G, Galluzzi V, Silva E. Directional pinning and anisotropy in $YBa_2Cu_3O_{7-x}$ with $BaZrO_3$ nanorods: Intrinsic and nanorods-induced anisotropy Physica C 503:146–149, 2014.
[57] Bothner D, Gaber T, Kemmler M, Koelle D, Kleiner R. Improving the performance of superconducting microwave resonators in magnetic fields Appl. Phys. Lett. 98:102504, 2011.
[58] Jin BB, Zhu BY, Wördenweber R, de Souza Silva CC, Wu PH, Moshchalkov VV. High-frequency vortex ratchet effect in a superconducting film with a nanoengineered array of asymmetric pinning sites Phys. Rev. B 81:174505, 2010.
[59] Wördenweber R, Hollmann E, Schubert J, Kutzner R, Panaitov G. Regimes of flux transport at microwave frequencies in nanostructured high-T_c films Phys. Rev. B 85:064503, 2012.
[60] Cuadra-Solis PdJ, Garcia-Santiago A, Hernandez JM, Tejada J, Vanacken J, Moshchalkov VV. Observation of commensurability effects in a patterned thin superconducting Pb film using microwave reflection spectrometry Phys. Rev. B 89:054517, 2014.
[61] Lara A, Aliev FG, Silhanek AV, Moshchalkov VV. Microwave-stimulated superconductivity due to presence of vortices Sci. Rep. 5:9187, 2015.
[62] Dobrovolskiy OV, Franke J, Huth M. ^{4}He sample probe for combined microwave and dc transport measurements Meas. Sci. Technol. 26:035502, 2015.
[63] Gittleman JI, Rosenblum B. The pinning potential and high-frequency studies of type-ii superconductors J. Appl. Phys. 39:2617–2621, 1968.
[64] Shklovskij VA, Dobrovolskiy OV. Microwave absorption by vortices in superconductors with a washboard pinning potential. In: Gabovich A (ed). Superconductors – Materials, Properties and Applications. InTech, Rijeka, 263–288, 2012.
[65] Lu Q, Reichhardt C J O Reichhardt C. Reversible vortex ratchet effects and ordering in superconductors with simple asymmetric potential arrays Phys. Rev. B 75:054502, 2007.
[66] Brandt EH. Linear a.c. response of high-Tc superconductors and the irreversibility line Physica Scripta 1992:63, 1992.
[67] Silva E, Pompeo N, Sarti S, Amabile C. Vortex state microwave response in superconducting cuprates Recent Developments in Superconductivity Research. Nova Science, Hauppauge, NY, 201–243, 2006.
[68] Dobrovolskiy OV. AC quantum interference effects in nanopatterned Nb microstrips J. Supercond. Nov. Magnet. 28:469–473, 2015.
[69] Shapiro S. Josephson currents in superconducting tunneling: The effect of microwaves and other observations Phys. Rev. Lett. 11:80–82, 1963.

[70] Fiory AT. Quantum interference effects of a moving vortex lattice in Al films Phys. Rev. Lett. 27:501–503, 1971.
[71] Fiory AT. Interference effects in a superconducting aluminum film; vortex structure and interactions Phys. Rev. B 7:1881–1889, 1973.
[72] Martinoli P, Daldini O, Leemann C, Van den Brandt B. Josephson oscillation of a moving vortex lattice Phys. Rev. Lett. 36:382–385, 1976.
[73] Martinoli P, Daldini O, Leemann C, Stocker EAC. quantum interference in superconducting films with periodically modulated thickness Solid State Commun. 17:205–209, 1975.
[74] Van Look L, Rosseel E, Van Bael MJ, Temst K, Moshchalkov VV, Bruynseraede Y. Shapiro steps in a superconducting film with an antidot lattice Phys. Rev. B 60:R6998–R7000, 1999.
[75] Van de Vondel J, Gladilin VN, Silhanek AV, Gillijns W, Tempere J, Devreese JT, Moshchalkov VV. Vortex core deformation and stepper-motor ratchet behavior in a superconducting aluminum film containing an array of holes Phys. Rev. Lett. 106:137003, 2011.
[76] Zeljko J, Milosevic M, Silhanek AV, Van de Vondel J. Stroboscopic phenomena in superconductors with dynamic pinning landscape Sci. Rep 5:14604, 2015.
[77] Thorne RE, Hubacek JS, Lyons WG, Lyding JW, Tucker JR. ac-dc interference, complete mode locking, and origin of coherent oscillations in sliding charge-density-wave systems Phys. Rev. B 37:10055–10067, 1988.
[78] Kriza G, Quirion G, Traetteberg O, Kang W, Jérome D. Shapiro interference in a spin-density-wave system Phys. Rev. Lett. 66:1922–1925, 1991.
[79] Sivakov AG, Glukhov AM, Omelyanchouk AN, Koval Y, Müller P, Ustinov AV. Josephson behavior of phase-slip lines in wide superconducting strips Phys. Rev. Lett. 91:267001, 2003.
[80] Reichhardt C, Reichhardt CJO. Shapiro steps for skyrmion motion on a washboard potential with longitudinal and transverse ac drives Phys. Rev. B 92:224432, 2015.
[81] Dobrovolskiy OV. Abrikosov fluxonics in washboard nanolandscapes Physica C 533:80, 2017.
[82] Plourde BLT. Nanostructured superconductors with asymmetric pinning potentials: Vortex ratchets IEEE Trans. Appl. Supercond. 19:3698–3714, 2009.